JAST, Vol. 7, No. 1, pp 9–17

JAST
Journal of Aerospace Science and Technology

Numerical Simulation of Fluid Flow Past a Square Cylinder Using a Lattice Boltzmann Method

S. Rowghani[1], M. Mirzaei[2], R. Kamali[3]

The method of Lattice Boltzmann Equation (LBE) is a kinetic-based approach for fluid flow computations. In the last decade, minimal kinetic models, primarily the LBE, have met with significant success in the simulation of complex hydrodynamic phenomena, ranging from slow flows in grossly irregular geometries to fully developed turbulence, to flow with dynamic phase transitions. In the present work, a computer code based on the Lattice Boltzmann Method (LBM) has been developed to show the capability of the method for simulating fluid flows. The confined flow around a cylinder with square cross-section mounted inside a plane channel (blockage ratio B=1/8) was investigated in detail with the LBM. The largest Reynolds number chosen was Re=300 based on the maximum inflow velocity and the chord length of the square cylinder. The LBE was built up on the basis the D2Q9 model and the single relaxation time method called the lattice-BGK method. Both velocity profiles and integral parameters such as drag coefficient and Strouhal number were investigated.

NOMENCLATURE

f	single particle mass distribution function
ξ	particle velocity vector
u	fluid velocity
p	pressure
x	spatial position vector
$f^{(0)}$	equilibrium distribution function
f_α	post-collision distribution function
λ	relaxation time
R	gas constant
T	gas temperature
ν	kinematic viscosity
e_α	discrete particle velocity in LBE model
w_α	weighting factor
$f_\alpha^{(eq)}$	equilibrium distribution function in discretized particle velocity space
$f_\alpha^{(neq)}$	none-equilibrium distribution function in discretized particle velocity space
c_s	speed of sound
δt	time step
δx	space step
τ	dimensionless relaxation time in LBGK
ϵ	Knudsen number

1. *Corresponding Author, MSc. Student, Aerospace Eng., Dept. of K.N. Univ. of Tech., Tehran, Iran, Email:sina_rowghani@yahoo.com.*
2. *Associate Professor, Aerospace Eng., Dept. of K.N. Univ. of Tech., Tehran, Iran, Email:mirzaei@kntu.ac.ir*
3. *Assistant Professor, Dept. of Mechanical Eng., Shiraz Univ., Shiraz, Iran.*

INTRODUCTION

In the last 15 years or so, there has been rapid progress in developing the method of the lattice Boltzmann equation (LBE) for solving a variety of fluid dynamic problems [1–6]. Historically, the LBE method was developed from the method of Lattice Gas Automata (LGA); see [7–11] for details on the LGA method. Nevertheless, the LBE method can be better appreciated by considering the Boltzmann equation directly. Adopting the macroscopic method for computational fluid dynamics (CFD), the macroscopic variables of interest such as velocity, u, and pressure, p, are usually obtained by solving the Navier–Stokes (NS) equations. In the LBE approach, one solves the kinetic equation

for the particle velocity distribution function $f(x, \xi, t)$ in which ξ is the particle velocity vector, x is the spatial position vector, and t is the time. A popular kinetic model adopted in the literature is the single-relaxation-time (SRT) approximation, the so-called Bhatnagar–Gross–Krook (BGK) model [12].

In contrast to the overwhelming number of publications on the flow past circular cylinders, the square counterpart has not been investigated extensively, although it plays a dominant role in many technical applications such as building aerodynamics. Depending on the Reynolds number, different flow regimes can be distinguished for a square cylinder[13]. At very small Reynolds numbers (Re<1), viscous forces dominate the flow. For this creeping flow, no separation takes place at the surface of the cylinder. With increasing Re, the flow separates first at the trailing edges of the cylinder and a closed steady recirculation region consisting of two symmetric vortices is observed behind the body. The size of the recirculation region increases with an increase in Re. When a critical Reynolds number Re_{crit}, is exceeded, the well-known von Karman vortex street with periodic vortex shedding from the cylinder can be detected in the wake. Different values of Re_{crit}, exist in the literature. Based on experimental investigations, Okajima [14] found periodic vortex motion at Re˜70 leading to an upper limit of Re_{crit}= 70. A smaller value (Re_{crit} = 54) was determined by Klekar and Patankar [15] based on a stability analysis of the flow. When the Reynolds number is further increased, the flow separates at the leading edges of the cylinder. The onset of this phenomenon is not clearly defined in the literature; only a wide range of Re=100 to 150 is given ([13],[14]). In this Reynolds number range, the flow past square cylinders can still be considered as 2D. In contrast to the circular cylinder flow for which Williamson [16] provides a Reynolds number limit of Re≈180 for the onset of 3D structures in the wake, no such clear statement can be found for the square counterpart. A rough hint is given by [13] with Re=300. Therefore, this Reynolds number was chosen as the upper limit of the present 2D laminar simulations. Beyond this limit, 3D structures have to be expected and subsequently transition to turbulence takes place in the free shear layers. In comparison with the free flow case, two new parameters have to be taken into account: the inflow profile and the blockage ratio. As shown by Davis *et.al.* [17], the vortex shedding frequency depends strongly on the inflow profile. In the experimental investigations by Shair *et.al.* [18] and [17], non-negligible deviations between the velocity profiles far upstream of the cylinder and the parabolic distribution expected for fully developed laminar channel flow were observed. Therefore, this aspect has to be kept in mind for comparison between experimental and numerical investigations which typically apply the theoretical velocity profile as inflow conditions. The second parameter which plays a dominant role in the confined cylinder flow is the blockage ratio of the channel, defined as $B = D/H$ where D is the diameter of the cylinder and H is the channel height. It is generally accepted that for a fixed Reynolds number, an increasing blockage ratio leads to an increase in the Strouhal number. This holds true for both circular and square cylinders, although the movement of the separation points cannot be responsible for this phenomenon for a sharp-edged body as assumed for a round geometry. Davis *et.al.* [17] investigated the confined flow past square cylinders for a wide range of Re and two different blockage ratios (B = 1/6 and 1/4) experimentally and numerically. Depending on the blockage ratio, a maximum Strouhal number was observed at Re=Re_{max} =200 to 350. For higher Re, the Strouhal number decreases again and reaches an almost constant level. As mentioned above, non -parabolic velocity profiles were measured upstream of the cylinder. Because most numerical predictions were based on these measured inflow profiles, a direct comparison with the present study is possible only for the additional cases in which a parabolic profile was assumed. These computations were based on a finite-volume code and non-equidistant coarse grids of 76 × 42 and 76×52 grid points. Two-dimensional numerical simulations were also carried out by Mukhopadhyay *et.al.* [19] for the Re range 90-1200, two blockage ratios (B =1/8 and 1/4) and a parabolic inflow profile. With respect to the Reynolds number of the corresponding channel flow, the upper limit of Re in this investigation seems to be highly questionable because a turbulent flow in the channel has to be expected under these conditions. For a blockage ratio B =1/5, Suzuki *et.al.* [20] computed Strouhal numbers over a wide Re range and found a maximum at Re=Re_{max} =150. Liu *et.al.* [21] solved the three dimensional cylinder in a channel using the LBM. A comparison of the different data mentioned above shows a large array of the results already for integral parameters such as the Strouhal number. There is evidently a lack of reliable experimental and numerical data for this flow case.

The objective of the present study was to yield a contribution to close this gap. The results were evaluated in detail based on velocity fields and integral parameters and compared with previous numerical and experimental studies. Therefore, besides the physics of the flow past a square cylinder, the paper focuses on the comparison of the accuracy of both methods. Moreover, one of the main features of the present study which makes it deferent from other similar works such as the work done by Breuer *et.al.* [29], is implementation of boundary conditions specially at the outlet of the channel. In fact, we tried various boundary conditions and we found a proper condition on this

boundary. Breuer *et.al.* [29] have used extrapolation method to calculate the velocity components at the outlet of the channel whereas in the present work we concluded that a combination of the extrapolation method and conservation of mass at this boundary accelerate the convergence rate.

DESCRIPTION OF NUMERICAL METHOD

A popular kinetic model adopted in the literature is the single-relaxation-time (SRT) approximation, the so-called Bhatnagar–Gross–Krook (BGK) model [12]:

$$\frac{\delta f}{\delta t} + \xi.\nabla f = -\frac{1}{\lambda}(f - f^{(0)}) \tag{1}$$

where $f^{(0)}$ is the equilibrium distribution function (the Maxwell–Boltzmann distribution function), and λ is the relaxation time. The corresponding viscosity is $\nu = \lambda RT$ in which R is the gas constant and T is the gas temperature. To solve for f numerically, Eq. (1) is first discretized in the velocity space using a finite set of velocity vectors $\{\ \xi_\alpha\}$ in the context of the conservation laws [22,23]:

$$\frac{\delta f_\alpha}{\delta t} + \xi_\alpha.\nabla f_\alpha = -\frac{1}{\lambda}(f_\alpha - f_\alpha^{(eq)}) \tag{2}$$

In the above equation, $f_\alpha(x,t) \equiv f_\alpha(x,\xi_\alpha,t)$ is the distribution function associated with the αth discrete velocity ξ_α and $f_\alpha^{(eq)}$ is the corresponding equilibrium distribution function in the discrete velocity space. The nine-velocity square lattice model, which is often referred to as the 2-D 9-velocity, D2Q9 model (Figure 1), has been widely and successfully used for simulating two-dimensional (2-D) flows. In the D2Q9 model, e_α denotes the discrete velocity set, namely:

$$\begin{aligned}
&e_0 = 0,\\
&e_\alpha = c(\cos((\alpha-1)\pi/4), \sin(\alpha-1)\pi/4)),\\
&\qquad for\ \alpha = 1,3,5,7,\\
&e_\alpha = \sqrt{2}c(\cos((\alpha-1)\pi/4), \sin(\alpha-1)\pi/4)),\\
&\qquad for\ \alpha = 2,4,6,8.
\end{aligned} \tag{3}$$

where $c = \delta x/\delta t$, δx and δt are the lattice constant and the time step size, respectively. The equilibrium distribution for D2Q9 model is of the form

$$f_\alpha^{(eq)} = \rho w_\alpha \left[1 + \frac{3}{c^2}e_\alpha.u + \frac{9}{2c^4}(e_\alpha.u)^2 - \frac{3}{2c^2}u.u\right] \tag{4}$$

where w_α is the weighting factor given by:

$$w_\alpha = \begin{cases} 4/9, & \alpha = 0\\ 1/9, & \alpha = 1,3,5,7\\ 1/36, & \alpha = 2,4,6,8 \end{cases} \tag{5}$$

In the discretized velocity space, the density and momentum fluxes can be evaluated as:

$$\rho = \sum_{x=0}^{8} f_\alpha = \sum_{x=0}^{8} f_\alpha^{(eq)} \tag{6}$$

and

$$\rho u = \sum_{x=1}^{8} e_\alpha f_\alpha = \sum_{x=1}^{8} e_\alpha f_\alpha^{(eq)} \tag{7}$$

The speed of sound in this model is $c_s = c/\sqrt{3}$ [24] and the equation of state is that of an ideal gas,

$$p = \rho.c_s^2 \tag{8}$$

Qian *et.al.* [24] also developed various models for 3-D flows with $f_\alpha^{(eq)}$ given in the same form as in Eq. (4). Depending on the number of the lattice velocity vectors used in these models, they are referred as D3Q15, D3Q19, and D3Q27 models. Eq. (2) is called the discrete velocity model (DVM). Numerically, it can be solved using any standard, practical method such as finite difference. In using finite difference formulation, one needs to be careful about reducing the numerical diffusion associated with the discretization of the advection term and the stiffness of the differential equation when λ<<1 is required for low viscosity flows. In the LBE method, Eq. (2) is discretized in a very special manner. The completely discretized equation, with the time step δt and space step $\delta x = e_\alpha.\delta t$, is:

$$\begin{aligned}
&f_\alpha(x_i + e_\alpha\delta t, t+\delta t) - f_\alpha(x_i,t)\\
&\qquad = -\frac{1}{\tau}\left[f_\alpha(x_i,t) - f_\alpha^{(eq)}(x_i,t)\right]
\end{aligned} \tag{9}$$

where $\tau = \lambda/\delta t$, and x_i is a point in the discretized physical space. Eq. (9), termed the LBE with BGK approximation or LBGK model, is usually solved in the following two steps:

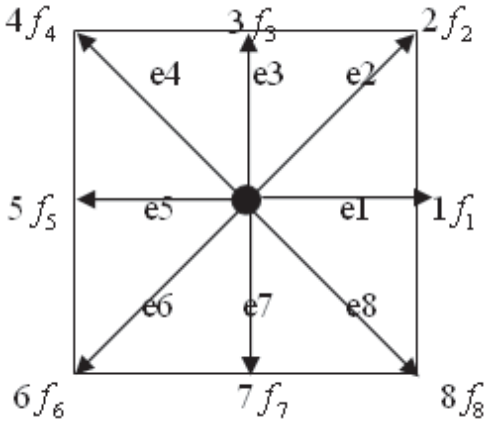

Figure 1. A 2-D 9-velocity lattice (D2Q9) model.

Collision step:

$$\tilde{f}_\alpha(x_i, t+\delta t) = f_\alpha(x_i, t) - \frac{1}{\tau}\left[f_\alpha(x_i, t) - f_\alpha^{eq}(x_i, t)\right] \tag{10a}$$

Streaming step :

$$f_\alpha(x_i + e_\alpha \delta t, t+\delta t) = \tilde{f}_\alpha(x_i, t+\delta t) \tag{10b}$$

where $\tilde{f}_\alpha$ represents the post-collision state. It needs to be emphasized that with such a splitting in the computational procedure, there is no need to store both $f_\alpha(x_i, t+\delta t)$ and $f_\alpha(x_i, t)$ during the computation. Information on one time level is sufficient for unsteady flow simulations. In order to derive the NS equations from LBE, the Chapman–Enskog expansion [25] is used. In essence, it is a standard multi-scale expansion, with time and space being rescaled as:
$t_1 = \epsilon t, \quad t_2 = \epsilon^2 t, \quad x_1 = \epsilon x,$

$$\frac{\partial}{\partial t} = \epsilon\frac{\partial}{\partial t_1} + \epsilon^2\frac{\partial}{\partial t_2}, \frac{\partial}{\partial x} = \epsilon\frac{\partial}{\partial x_1} \tag{11}$$

and the particle distribution function f_α expanded as:

$$f_\alpha = f_\alpha^{(0)} + \epsilon f_\alpha^{(1)} + \epsilon^2 f_\alpha^{(2)} + O(\epsilon^3). \tag{12}$$

In the incompressible flow limit, $|u|/c_s^2 << 1$, the conservation principles of mass and momentum yield:

$$\frac{\partial u_\alpha}{\partial x_\alpha} = 0, \tag{13}$$

$$\frac{\partial u_\alpha}{\partial t} + u_\beta\frac{\partial u_\alpha}{\partial x_\beta} = -\frac{1}{\rho}\frac{\partial p}{\partial x_\alpha} + v\nabla^2 u_\alpha. \tag{14}$$

The corresponding viscosity in the NS equation (14) derived from Eq. (9) is [24]:

$$v = (\tau - 1/2)c_s^2\delta t. \tag{15}$$

The modification of viscosity (from $\nu = \lambda.c_s^2$ in Eq. (1)) corrects for the truncation error in the discretization of Eq. (2) and formally makes the LBGK scheme a second order method for solving incompressible flows [26]. The positivity of the viscosity requires that $\tau > \frac{1}{2}$ in all LBE computations. It is noted that the pressure p is obtained through an equation of state (Eq. (8)). The collision step is completely local. The streaming step involves no computation. Eq. (9) is explicit, easy to implement, and straightforward to parallelize.

DETAILS OF THE TEST CASE

Geometry of the computational domain and grids

The 2D laminar flow around a square cylinder with diameter D mounted centered inside a plane channel (height H) was investigated (see Figure 2). The blockage ratio was fixed at $B = 1/8$. In order to reduce the influence of inflow and outflow boundary conditions, the length of the channel was set to $L/D = 50$. The inflow length was fixed to $l = L/4$.

The LBA method allows the application of simple orthogonal equidistant lattices/grids. This lattice type makes (semiautomatic) integration of arbitrary, complex geometries very easy: single lattice nodes are either occupied by an elementary obstacle or they are free (marker and cell approach). The simulation was carried out by three different grids, namely 500×80, 1000×160 and 2000×320. The number of lattice nodes on each side of the square cylinder varies between 10 and 40.

Boundary conditions

It is often argued that the so-called 'bounce back' wall boundary conditions, which are also used in the present implementation of the LBA scheme, are of first-order accuracy, whereas the lattice-Boltzmann equation is of second-order. However, recent investigations showed that the error produced by the bounce back boundary condition is sufficiently small if the relaxation parameter ω is close enough to 2 (Inamuro *et.al.* [27]), allowing a precise knowledge of the wall position with zero flow velocity.

Bounce back boundary condition is the most efficient one for arbitrary, complex geometries, which are most typical for the application of the LBM.

By the so-called bounce back scheme, we mean that when a particle distribution streams to a wall

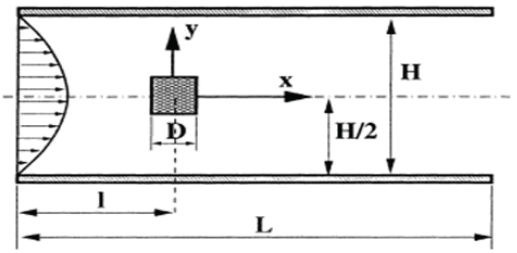

Figure 2. Definition of the geometry and integration domain.

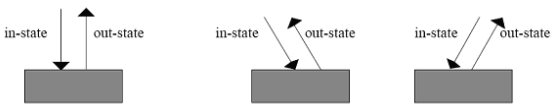

Figure 3. Bounce back scheme.

node, the particle distribution scatters back to the node it came from (Figure 3).

For a node near a boundary, some of its neighboring nodes lie outside the flow domain. Therefore, the distribution functions at these no-slip nodes are not uniquely defined. The bounce back scheme is a simple way to fix these unknown distributions on the wall node.

In order to simulate a fully developed laminar channel flow upstream of the square cylinder, a parabolic velocity profile with a maximum velocity $u_{\max}$ is prescribed at the channel inlet. This velocity was chosen to be lower than 10% of the speed of sound for the LBA simulations to avoid significant compressibility effects which are known to increase with the square of the Mach number. For the LBA, the pressure at the inlet is extrapolated upstream, and the equilibrium density distribution (Eq. (3)) was computed from that pressure and the given velocity and imposed at the first lattice column.

On the outlet, a fixed pressure is imposed in terms of the equilibrium distribution function. For this task, the velocity components are calculated based on a combination of extrapolated downstream and conservation of mass. This condition leads to higher convergence rate in comparison to pure extrapolation method.

RESULTS AND DISCUSSION

A Reynolds number range $0.5 \leq \mathrm{Re} \leq 300$ was investigated numerically, where Re is based on the cylinder diameter D and the maximum flow velocity $u_{\max}$ of the parabolic inflow profile. The following section starts with a description of the different flow patterns observed with increasing Re. The subsequent sections present a detailed comparison of the computed results based on velocity profiles at several positions in the flow field. Furthermore, the computations are analyzed and compared regarding integral flow parameters such as Strouhal number and dimensionless force coefficients (drag).

Flow pattern

Figure 4 shows computational results in the vicinity of the cylinder by streamlines at four different Reynolds numbers (Re=1, 30, 60, 200), each characterizing a totally different flow regime.

At low Re=1, the creeping steady flow past the square cylinder persists without separation (Figure 4(a)). The magnitude of viscous forces decreases with increasing Re until a certain value, at which separation of the laminar boundary layers occurs. In comparison with the circular counterpart, for which a value of Re=5 was found (Zdravkovich [28]), separation at the trailing edges of the sharp-edged body can be observed at lower Re. Above this limit, the wake comprises a

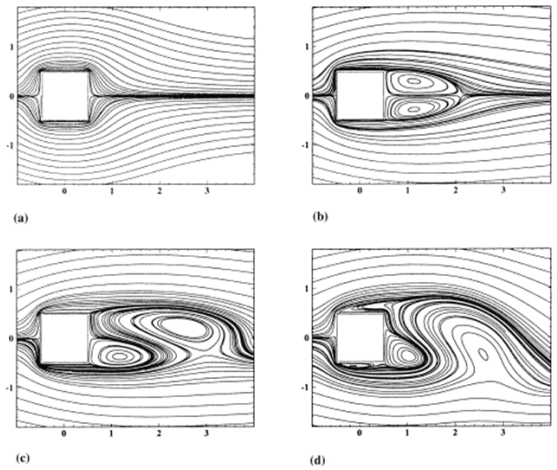

Figure 4. Streamlines around the square cylinder for different Reynolds numbers (a) Re=1; (b) Re= 30; (c) Re=60; (d) Re= 200.

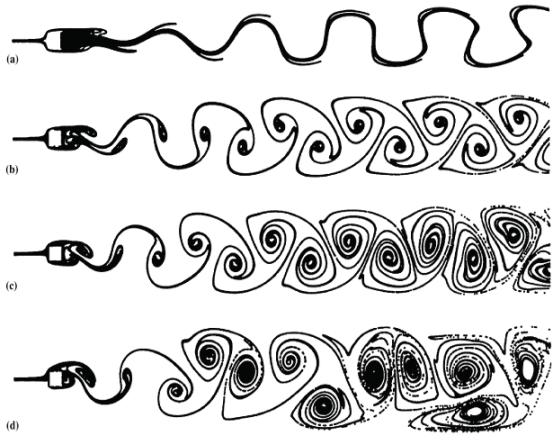

Figure 5. Streaklines around the square cylinder for different Reynolds numbers (a) Re=60; (b) Re=100; (c) Re=200; (d) Re=300.

steady recirculation region of two symmetrically placed vortices on each side of the wake, as shown in Figure 4(b) at Re=30, whose length grows as Re increases. The same trend was observed for circular cylinders. Owing to the sharp corners, the separation point is fixed at the trailing edge and the flow is attached at the side walls. The steady, elongated and closed near-wake becomes unstable when $\mathrm{Re} > \mathrm{Re}_{crit}$ (Figure 4(c)). The transverse oscillation starts at the end of the near-wake and initiates a wave along the trail. This phenomenon is visualized by streaklines in Figure 5(a) (Re=60). Weightless particles released at different sources in front of the cylinder were integrated during the time-dependent flow computation. As stated earlier, Klekar and Patankar determined a critical value of $\mathrm{Re}_{crit} = 54$. Although this limit depends on flow parameters such as the blockage ratio, a similar value ($\mathrm{Re}_{crit} \approx 60$) was observed in the present computations. When Re is

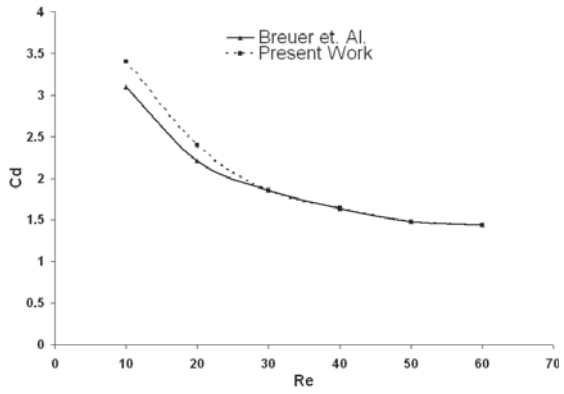

Figure 6. computed drag coefficient vs. Reynols number.

further increased, the free shear layers begin to roll up and form eddies as shown in Figure 5(b) at Re=100. This phenomenon is well known as the von Karman vortex street.

The wavelength of vortex shedding decreases with rising Re, as seen in Figure 5. Another important change in the flow structure is observed in the range Re=100 to 150, where separation already starts at the leading edge of the cylinder (Figure 4 (d), Re=200). As will be seen below, this strongly influences the frequency of vortex shedding. The upper limit of this laminar 2D shedding has an enormous spread in the literature. Preliminary 3D simulations have shown that the flow computation shown in Figure 5(d) at Re=300 is slightly beyond the limit where 2D simulations can be carried out. The deviations from fully periodic structures in the far-wake are also a clear hint for this statement.

Furthermore, it should be taken into account that the Reynolds number based on the channel height H and the mean velocity u_{mean} in the channel is already $\mathrm{Re}_{channel} = 1600$ for this case. Therefore, owing to the triggering effect of the obstacle on the channel flow, transition to turbulence has to be expected leading to 3D structures in the wake.

Steady flow: $0.5 \leq \mathrm{Re} < 60$

Drag coefficient

One of the most important characteristic quantities of the flow around a cylinder is the drag coefficient C_d. In the region of small Reynolds numbers, the drag coefficient varies strongly with Re. The contributions of the viscous and pressure forces to the total drag are of the same order of magnitude. A comparison of the computed LBM results is shown in Figure 6 for the steady-state results in the range $0.5 \leq \mathrm{Re} \leq 60$.

The difference between the LBA and FVM results occurs for small Reynolds numbers, whereas the agreement for the upper Re range considered is satisfactory. As the discrepancies are larger in the lower Re range, where the viscous forces play a dominant role for the drag, it can be concluded that an insufficient resolution of the boundary layers by the LBA method is responsible for this behavior.

Unsteady flow: 60<Re<300

Velocity profiles

The results of this part is limited to Re=100. As the flow is unsteady at this Reynolds, it is necessary to define the time of evaluation. This is given by the time level at which the cross stream velocity V at an axial position of $10D$ behind the cylinder changes its sign from minus to plus.

Figure 7 shows the velocity distribution of both velocity components along the centerline.

Figure 8 shows velocity profiles of U and V at three different axial positions, x=0, 4 and 8. For the profile through the center of the cylinder (x=0), no deviations are visible between the two sets of results. For

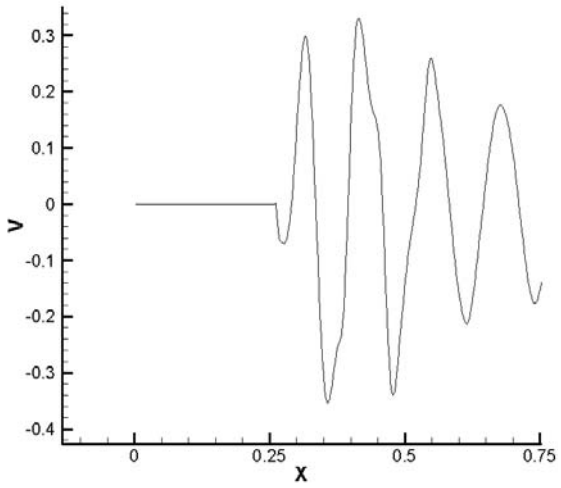

(a)

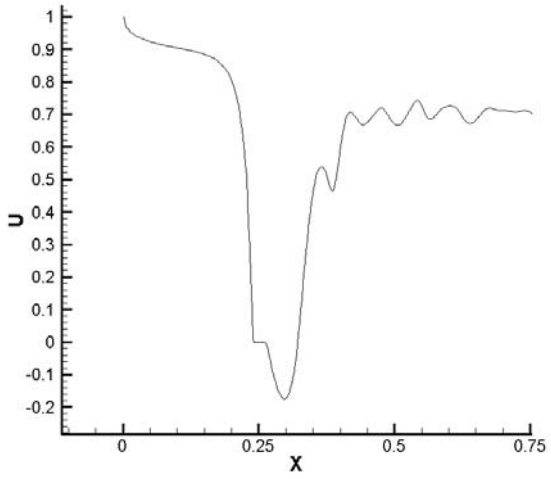

(b)

Figure 7. (a) streamwise (U) and (b) cross-stream (V) velocities along the centerline ($y = 0$), Re=100.

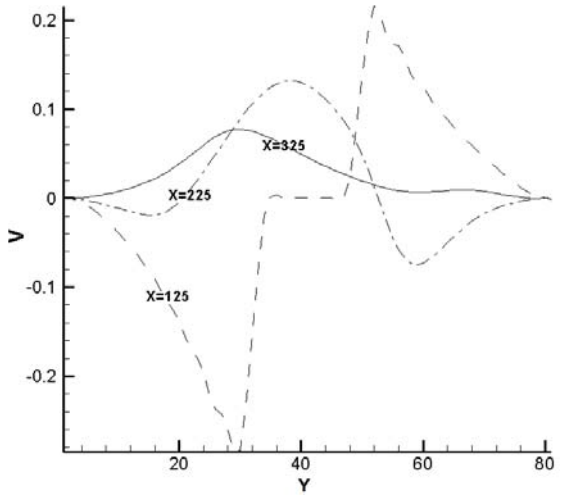

(a)

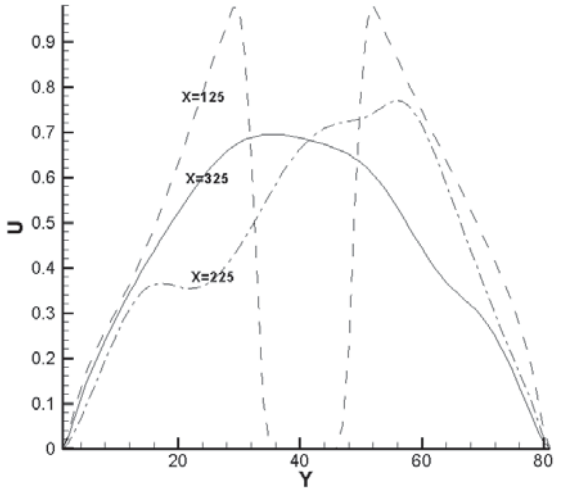

(b)

Figure 8. (a) streamwise (U) and (b) cross-stream (V) velocities at three different positions in the flow field, center of cylinder ($x = 0$), near-wake ($x = 4$) and far-wake ($x = 8$), Re=100.

the assessment of the agreement between the results of the different numerical methods, it should be taken into account that the flow is very unsteady. Therefore, the definition of the moment of evaluation has a strong influence on the results. Owing to finite time steps (and also finite spatial resolution), the accuracy in time in the worst case is one time step size. Therefore, an exact agreement between the computational results cannot be expected.

Strouhal number

One important quantity taken into account in the present analysis is the Strouhal number St, computed from the cylinder diameter D, the measured frequency of the vortex shedding f and the maximum velocity $u_{\max}$ at the inflow plane $St = fD/u_{\max}$.

The characteristic frequency f was determined by a spectral analysis (fast Fourier transformation, FFT) of time series of the lift coefficient Cl. Figure 9 shows the computational results.

It shows an increase in the Strouhal number with increasing Re. At the upper limit of this range, an important change in the flow structure takes place, namely the movement of the separation point from the trailing edge to the leading edge of the square cylinder. As expected, the separation on the side walls is strongly influenced by the resolution in the vicinity of the body. Therefore, the results of the coarsest grid with only 10 points on each surface do not have to be discussed seriously. At the finest resolution, each side of the cylinder is represented by 40 nodes with a smallest distance to the wall of $0.025D$. The Strouhal number has a maximum at about Re=150 to 160 and decreases again for higher Re.

Drag coefficient

In the unsteady 2D flow regime ($60 \leq \mathrm{Re} \leq 300$), the nearwake becomes unstable and a sinusoidal oscillation

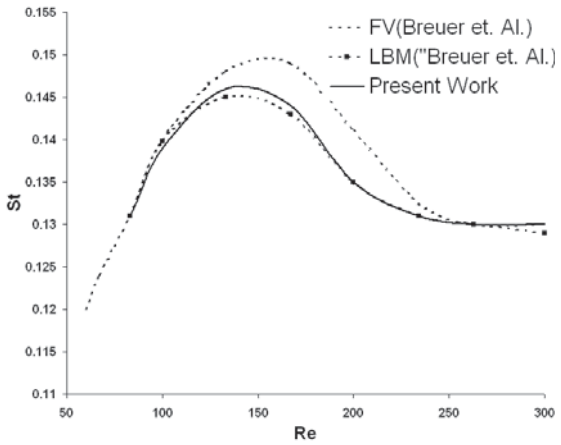

Figure 9. Computed Strouhal numbers vs. Reynolds number.

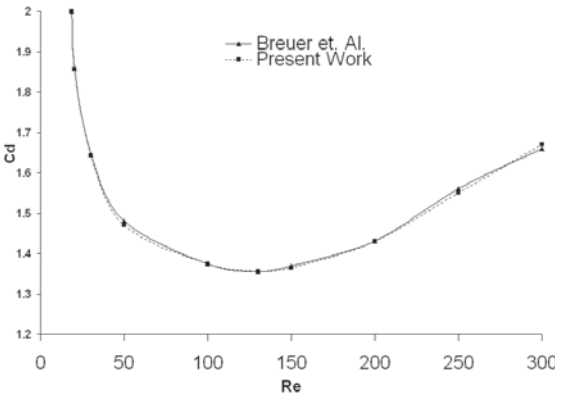

Figure 10. Computed drag coefficient Cd vs. Reynolds number for unsteady flow.

of the shear layers commences, later forming the von Karman vortex street. In Figure 10, the time-averaged drag coefficients in this Re range are plotted. The Cd-Re curve has a local minimum at Re $\approx$ 150.

No experimental or other numerical data for comparison were found in the literature for the same inflow conditions and blockage ratio. However, at least the computations of Franke (1991) and Franke *et.al.* (1990) for a square cylinder under free stream conditions confirm our finding of a local Cd minimum approximately at the Reynolds number where separation is initiated at the leading edge.

CONCLUSIONS

A lack of accurate and detailed data was found in the literature for the confined laminar flow past a square cylinder, which initiated the present work. In order to generate reliable numerical results, The LBM was applied to investigate the 2D flow past a square cylinder inside a channel ($B = 1/8$) for the Reynolds number range $0.5 \leq \mathrm{Re} \leq 300$. For steady flow (Re<60), small deviations were detected for the drag coefficients in the lower Re range. The unsteady flow computations impressively demonstrate the capability of the LBA to deal with instantaneous flows. Velocity profiles at different locations in the flow field (Re=100) were evaluated. Strouhal numbers were determined for the entire Reynolds number range. Both methods provide a local maximum of St at Re=150. Compared with the scattered data in the literature, the deviations between the LBA and FVM results are almost negligible. Finally, drag coefficients were computed and compared. As is known from the literature for square cylinders in free stream, the drag coefficient of a con- fined cylinder also shows a local minimum at Re=150. In conclusion, the present work provides reliable and accurate results for the confined cylinder flow which were not previously available. The extension to 3D computations and higher Reynolds numbers is the subject of further investigations within ongoing research.

REFERENCES

1. Alves A.S., "Discrete Models of Fluid Dynamics", *Figueira da Foz*, Portugal, (1990).
2. Boghosian B.M., "Proceedings of the Seventh International Conference on the Discrete Simulation of Fluids", *Int. J. Mod. Phys. C* , (1998).
3. Succi S., *The Lattice Boltzmann Equation for Fluid Dynamics and Beyond*, Oxford University Press, (2001).
4. Qian Y.H., Succi S., Orszag S.A., "Recent Advances in Lattice Boltzmann Computing. In: Stauffer D", *Annual Reviews of Computational Physics III*, (1996).
5. Chen S., Doolen G.D., "Lattice Boltzmann Method for Fluid Flows", *Ann. Rev. Fluid Mech.* , **30**, (1998).
6. Luo L-S. , "The Lattice-Gas and Lattice Boltzmann Methods: Past, Present, and Future", *Proceedings of the International Conference on Applied Computational Fluid Dynamics*, PP 52-83(2000).
7. Ohashi H., Chen Y., "Proceedings of the Eighth International Symposium on the Discrete Simulation of Fluid Dynamics", **129**(1-3), (1999).
8. Lebowitz J.L., "Special Issue Based on the Ninth Annual International Conference on Discrete Simulation of Fluid Dynamics", *J. Stat Phys.*, (2000).
9. Coveney P.V., Succi S., "Discrete Modelling and Simulation of Fluid Dynamics", *The 10th International Conference on Discrete Simulation of Fluid Dynamics*, PP 1-573(2001).
10. Monaco R, Preziosi L., "Fluid Dynamic Applications of the Discrete Boltzmann Equation", *Singapore: World Scientific*, (1991).
11. Chopard B., Droz M., *Cellular Automata Modeling of Physical Systems*, Cambridge University Press, (1998).
12. Bhatnagar P.L., Gross E.P., Krook M.A., "Model for Collision Processes in Gases, I. Small Amplitude Processes in Charged and Neutral One-Com Ponent System", *Phys. Rev.*, **94**, PP 511-25(1954).
13. Franke R., "Numerische Berechnung Der Instationaren Wirbelablosung Hinter Zylindrischen Korpern", Ph.D. Thesis, University of Karlsruhe, (1991).
14. Okajima A., "Strouhal Numbers of Rectangular Cylinders", *J. Fluid Mech.*, **123**, PP 379-398(1982).
15. Klekar K.M., Patankar S.V., "Numerical Prediction of Vortex Shedding Behind Square Cylinders", *Int. J. Numer. Meth. Fluids* , **14**, PP 327-341(1992).
16. Williamson C.H.K., "Vortex Dynamics in the Cylinder Wake", *Annu. Rev. Fluid Mech.*, **28**, PP 477-539(1996).
17. Davis R.W., Moore E.F., Purtell L.P., "A Numerical-Experimental Study of Confined Flow Around Rectangular Cylinders", *Phys. Fluids*, **27**(1), PP 46-59(1984).
18. Shair F.H., Grove A.S., Petersen E.E., Acrivos A., "The Effect of Confining Walls on the Stability of the Steady Wake Behind a Circular Cylinder", *J. Fluid Mech.*, **17**, PP 546-550(1963).
19. Mukhopadhyay A., Biswas G., Sundararajan T., "Numerical Investigation of Confined Wakes Behind a Square Cylinder in a Channel", *Int. J. Numer. Meth. Fluids* , **14**, PP 1473-1484(1992).
20. Suzuki H., Inoue Y., Nishimura T., Fukutani F., Suzuki K., "Unsteady Flow in a Channel Obstructed by a Square Rod (Crisscross Motion of Vortex)", *Int. J. Heat Fluid Flow* , **14**(1), PP 2-9(1993).
21. Liu Y., So R.M.C., Cui Z.X., "A Finite Cantilevered Cylinder in a Cross Flow", *Journal of Fluids and Structures*, **20**, PP 589-609(2005).
22. He X., Luo L-S., "A Priori Derivation of the Lattice Boltzmann Equation", *Phys. Rev. E* , **55**, (1997).

23. He X., Luo L-S., "Theory of the Lattice Boltzmann Equation: From Boltzmann Equation to Lattice Boltzmann Equation", *Phys. Rev. E* , **56**, (1997).
24. Qian Y.H., d'Humi"eres D., Lallemand P. , "Lattice BGK Models for Navier Stokes Equation", *Europhys. Lett.*, **17**, PP 479-84(1992).
25. Chapman S, Cowling T.G., "The Mathematical Theory of Nonuniform Gases", *Cambridge University Press*, (1970).
26. Inamuro T., Sturtevant B., "Numerical Study of Discrete Velocity Gases", *Phys. Fluids A* , **2**, PP 2196-203(1990).
27. Inamuro T., Yoshine M., Ogino F., "A Non-Slip Boundary Condition for Lattice Boltzmann Simulations", *Phys. Fluids*, **7**(12), PP 2928-2930(1995).
28. Zdravkovich M.M., "Flow Around Circular Cylinders, vol 1: Fundamentals", *Oxford University Press*, (1997).
29. Breuer M., Bernsdorf J., Zeiser T., Durst F., "Accurate Computations of the Laminar Flow Past a Square Cylinder Based on Two Different Methods: Lattice-Boltzmann and Finite-Volume", *International Journal of Heat and Fluid Flow*, **21**, PP 186-196(2000).